Sonochemistry of actinides: from ions to nanoparticles and beyond

Sergey Nikitenko, Matthieu Virot, Philippe Moisy

Sergey I. Nikitenko[1]*, Matthieu Virot[1] and Philippe Moisy[2]

Sonochemistry of actinides: from ions to nanoparticles and beyond

[1]ICSM, Univ Montpellier, UMR 5257, CEA-CNRS-UM-ENSCM, Marcoule, France

[2]CEA, DES, ISEC, DMRC, Univ Montpellier, Marcoule, France

*Corresponding author: serguei.nikitenko@cea.fr

Abstract: Sonochemistry studies chemical and physical effects in liquids submitted to power ultrasound. These effects arise not from a direct interaction of molecules with sound waves, but rather from the acoustic cavitation: the nucleation, growth, and implosive collapse of microbubbles in liquids submitted to power ultrasound. The violent implosion of bubbles leads to the formation of chemically reactive species. In principle, each cavitation bubble can be considered as a microreactor initiating chemical reactions at mild conditions. In addition, microjets and shock waves accompanied bubble collapse produce fragmentation, dispersion and erosion of solid surfaces or particles. Microbubbles oscillating in liquids also enable nucleation and precipitation of nanosized actinide compounds with specific morphology. This review focuses on the versatile sonochemical processes with actinide ions and particles in homogeneous solutions and heterogeneous systems. The redox reactions in aqueous solutions, dissolution or precipitation of refractory solids, synthesis of actinide nanoparticles, and ultrasonically driving decontamination are considered. The guideline for further research is also discussed.

1 Introduction

When studying the action of 100-500 kHz ultrasound on aqueous solutions Richards and Loomis [1] discovered that the ultrasonic waves accelerate the hydrolysis of dimethylsulfate and the reduction of potassium iodate by sulfurous acid (iodine "clock" reaction). Two years later, Schmitt et al. [2] reported the oxidation of iodide ions in aqueous solutions under the effect of 750 kHz ultrasound. These seminal works have introduced a new field of chemistry called as "sonochemistry" by Neppiras [3]. Large amount of research papers and detailed critical reviews have been published since that time describing different ultrasonic processes, such as cleaning and degassing [4], extraction of biologically active compounds [5], food processing [6, 7], advanced oxidation processes [8, 9], and synthesis of nanostructured materials [10].

The history of actinide chemistry in solutions submitted to power ultrasound traces back to the nineties of the last century. In 1991, Nikonov from the Russian Institute of Physical Chemistry has defended a seminal PhD thesis dedicated to this topic [11]. A basic idea to use power ultrasound for the control of actinide behavior has been originated from the fact that cavitation bubbles produced by the propagation of ultrasonic waves in fluid media exhibit chemical activity. The possible in-situ and room temperature generation of active species is somewhat similar to radiolysis or photolysis and therefore present a strong interest for the redox control of actinides in hydrometallurgical processes, without addition of side reagents [12, 13]. In contrast to the later chemical phenomena, power ultrasound in heterogeneous solid-liquid systems also provides strong mechanical effects, such as dispersion of solids, depassivation of surfaces, emulsification, acceleration of mass and heat transfer, etc. making ultrasound a powerful tool to enhance the reactivity or activate material surfaces [14]. More generally, sonochemistry provides an original, simple and robust approach that may limit the industrial

manipulation of radioactive solutions and decrease the volume of problematic wastes that require to be further treated by nuclear industry.

In 1994, Charles Madic has initiated the research of sonochemistry in French CEA, which resulted in two PhD theses defended by L. Venault [15] and F. Juillet [16] and dedicated to the sonochemistry of U and Pu in homogeneous nitric acid solutions and sonochemical dissolution of PuO_2, respectively. Many studies of actinide behavior under power ultrasound have been reported worldwide more recently. Since 2008, the sonochemistry of actinides is one of the topics of Marcoule Institute for Separation Chemistry (ICSM, France). The potential applications of sonochemistry in advanced nuclear fuel cycle have been summarized in two reviews of Nikitenko et al. [17] and Rubio et al. [18]. The first review highlighted sonochemical reactions of actinides in homogeneous nitric acid solutions. The second paper discussed how sonoprocessing could potentially add value to the process streams throughout the nuclear fuel cycle. The current review briefly considers actinide sonochemical reactions in homogeneous aqueous solutions and focuses on heterogeneous processes including dissolution and precipitation of actinide compounds, decontamination of solids polluted with radionuclides, and sonochemical formation of actinide nanoparticles.

2 Fundamental background of sonochemistry

2.1 Chemical and physical effects of cavitation bubbles

Ultrasound spans the frequencies of roughly 15 kHz to 1 GHz. However, the chemical effects of ultrasound are observed in the frequency range of ca. 15 kHz – 2 MHz. The acoustic wavelengths of chemically active ultrasound ($1\text{-}10^{-4}$ cm) are much higher than the molecule size. Therefore, sonochemistry does not arise from a direct action of ultrasonic waves on molecules or ions but is rather attributed to the acoustic cavitation phenomenon. Simply put, cavitation is a set of consequent events: nucleation, growth and violent implosive collapse of microbubbles formed in liquids submitted to ultrasonic vibrations. There is a consensus that the chemical and physical effects of power ultrasound are related to the extremely rapid implosion of the cavitation bubbles. On the other hand, the origin of the extreme conditions reached inside these cavities is still under debate. The mainstream concept of the chemical processes driven by power ultrasound is based on the idea of a quasi-adiabatic heating of the gas/vapor mixture inside the inertial cavitation bubbles (hot spot). In terms of hot spot approach, the inner core of the cavitation bubble shows a transient equivalent temperature of roughly 5000 K and pressures of 1000 bar at the last stage of the bubble collapse [19]. The strong local heating leads to the homolytic splitting of the molecular bonds yielding highly reactive radicals. However, recent studies of sonoluminescence spectroscopy revealed the formation of a non-equilibrium plasma inside the cavitation bubble [20]. Consequently, ionization processes inside the bubble should be taken into account as well. Besides the gas phase reaction zone, two other reaction sites are considered in sonochemistry: the interface between the bubble and the surrounding liquid where radical recombination and hydrothermal-like conditions have been described, and the bulk solution where chemically active species may migrate and react [8]. For the sonochemistry of actinides, these reaction zones are the most important. Therefore, plasmochemical reactions inside the bubble will not be discussed in this review.

It is important to emphasize that the acoustic cavitation is accompanied not only by the generation of chemically active species but also by strong mechanical forces arising from around violently imploding bubbles, which play a much more important role in heterogeneous systems than in homogeneous solutions. In addition to shock waves produced by the spherical bubble implosion, the micro-jets observed by the asymmetric bubble collapse at the vicinity of a solid/liquid interface provide intense pressure and temperature gradients in the local surrounding. Today, the use of power ultrasound to enhance the reactivity of solids has become a routine technique in heterogeneous catalysis and various cleaning and extraction processes [14]. In general, the mechanical effects of ultrasound are stronger at

low-frequency ultrasound (<100 kHz) compared to high ultrasonic frequency, which is related to the decrease of bubble size with the increase of ultrasonic frequency.

2.2 Sonolysis of water

It has been known since a long time that ultrasonic treatment enables the splitting of water molecules and formation of hydrogen gas and hydrogen peroxide in solution. Molecular hydrogen is formed by recombination of H atoms mostly inside the bubble and hydrogen peroxide is formed by recombination of $OH^{\bullet}$ radicals at the bubble/solution interface [21, 22]. It is worth noting that the formation of O_2 during water sonolysis has never been observed experimentally. In addition, the formation of H_2O_2 follows zero-order kinetics indicating that the limiting stage of the water splitting is a process occurring inside the bubble. Its efficiency and the related formation of reactive species is strongly influenced by experimental conditions, such as ultrasonic frequency, ultrasonic intensity or acoustic power, saturating gas, bulk temperature, and the presence of solid particles in solution as well. In general, the maximal yield of the sonochemical products is observed at ca. 300-400 kHz. There is actually no simple explanation of the effect of ultrasonic frequency on the sonochemical activity. According to literature [23], many parameters could affect reactivity in different ways. A faster rate of the cavitation events, larger number of active bubbles, and more extreme intrabubble conditions at high frequency would favorize chemical reactivity. On the other hand, a dramatic decrease of the resonance bubble size with ultrasonic frequency would lead to diminishing of global active volume generating radicals in sonicated solutions. However, longer collapse and larger bubble surface at low frequency would allow more chemical reactions to take place at bubble/solution interface. The optimal frequency for sonochemical products formation is defined by the superposition of these opposite phenomena.

The composition of the saturating gas is a key parameter determining the efficiency of sonochemical reactions. Figure 1 demonstrates that the maximal yield achieved for H_2O_2 sonochemical formation is reached in Ar/20%O_2 gas mixture compared to pure Ar or O_2 [24, 25]. The lowering of the reaction rate in pure oxygen has been attributed to the sonochemical plasma quenching by molecular oxygen. It is worth noting that the yield of H_2 is sharply decreased in the presence of O_2 due to the scavenging of H atoms. In general, the mechanism of sonochemical water splitting in the presence of O_2 can be described with the reactions (1-7) as follows:

$$H_2O \rightarrow))) \rightarrow H + OH^{\bullet} \quad (1)$$

$$O_2 \rightarrow))) \rightarrow 2\,O^{\bullet\bullet} \quad (2)$$

$$O^{\bullet\bullet} + H_2O \rightarrow 2\,OH^{\bullet} \quad (3)$$

$$H + O^{\bullet\bullet} \rightarrow OH^{\bullet} \quad (4)$$

$$O_2 + H \rightarrow HO_2^{\bullet} \quad (5)$$

$$2\,OH^{\bullet} \rightarrow H_2O_2 \quad (6)$$

$$2\,HO_2^{\bullet} \rightarrow H_2O_2 + O_2 \quad (7)$$

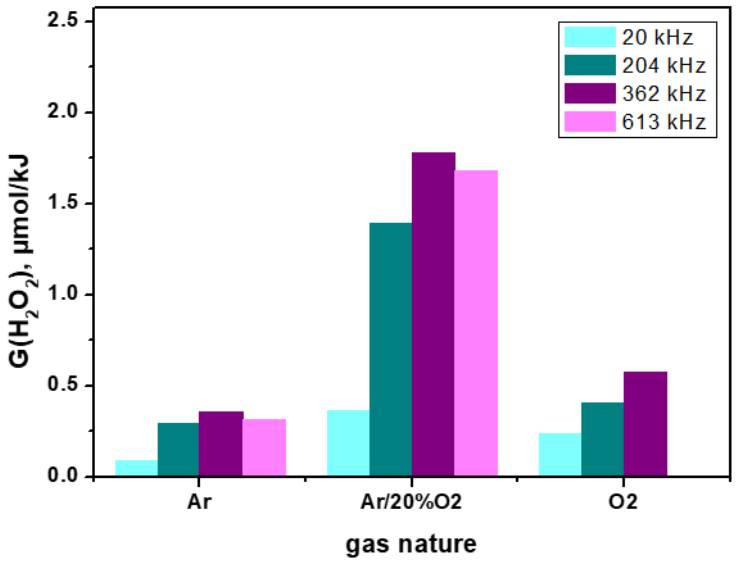

Figure 1: Effect of oxygen concentration on the sonochemical yield, G, of hydrogen peroxide during sonolysis of water. T= 20°C, gas bubbling at 80 mL·min^{-1}, no mechanical stirring. 20 kHz, P_{ac} = 33 W; 204 kHz, P_{ac} = 41 W; 362 kHz, P_{ac} = 43 W, 613 kHz, P_{ac} = 43 W. Reproduced from [25].

In the presence of air [26-29], Ar/N_2 [30], and Ar/N_2O [31], sonolysis of water leads to a quite complex mixture of products, such as HNO_2, HNO_3, NO, H_2O_2, and H_2. The ratio of the reaction yields for these products depends on the ultrasonic frequency and saturating gas. It is important to emphasize that the formation of nitrogen species indicates splitting of N_2 molecules inside the cavitation bubble along with H_2O molecules. Hart and Henglein [32] have shown that HNO_2 is not the main product of N_2O sonolysis in water. Instead, dissociation of N_2O causes mostly formation of N_2 and NO. In the presence of carbon monoxide, the yield of H_2O_2 is sharply decreased, but the yield of H_2 is raised [33]. The effect of CO has been explained by the scavenging of $OH^{\bullet}$ radicals formed during the sonochemical splitting of H_2O according to the reactions (8-9) below:

$$OH^{\bullet} + CO \rightarrow CO_2 + H \quad (8)$$

$$2H \rightarrow H_2 \quad (9)$$

2.3 Sonochemistry of aqueous nitric acid solutions

The processes observed in nitric acid solutions are of major importance for spent nuclear fuel reprocessing. Therefore, several papers have been devoted to the sonochemistry of nitric acid. In the absence of anti-nitrous reagents, ultrasonic treatment of aqueous nitric acid solutions causes the formation of nitrous acid and NO_x gases [34]. The kinetic curves of HNO_2 formation can be characterized by two stages. At the initial stage, HNO_2 is formed following zero-order kinetics. At the second stage, the concentration of HNO_2 reaches a steady-state and NO_x gases start to release from the sonicated solution as a result of its decomposition. Sonolysis of nitric acid has been attributed to the decomposition of volatile HNO_3 molecules inside the bubble and non-volatile NO_3^- ions at the bubble/liquid interface (reaction 10). Bubbling of NO, NO_2 [35] and N_2O [32] mixtures with Ar through sonicated HNO_3 solutions significantly influences HNO_2 formation rate. At low contents of NO and NO_2 in Ar (1.1-1.7 vol.%), 20 kHz ultrasound accelerates HNO_2 formation, which was attributed to their reactions with HNO_3 degradation products inside the bubbles and bubble/solution interface. By contrast, at higher contents of NO and NO_2, ultrasound has no influence on HNO_2 formation. The increase of HNO_2 formation rate with N_2O was explained by the dissociation of the latter inside the bubble and the subsequent reactions of formed $O^{\bullet\bullet}$ with NO arisen from HNO_3 sonochemical degradation (reactions 10-13):

$$2\ HNO_3 \rightarrow))) \rightarrow 2\ NO + H_2O + 3/2\ O_2 \quad (10)$$

$$N_2O \rightarrow))) \rightarrow N_2 + O^{\bullet\bullet} \quad (11)$$

$$NO + O^{\bullet\bullet} \rightarrow NO_2 \quad (12)$$
$$2\ NO_2 + H_2O \rightarrow HNO_2 + HNO_3 \quad (13)$$

Most likely, the reaction (13) occurs at the bubble/liquid interface. In such conditions, H_2O_2 does not accumulate due to its rapid reaction with HNO_2 according to the reaction (14). In the presence of anti-nitrous reagents, such as hydrazinium nitrate or sulfamic acid, the formation of H_2O_2 is clearly observed [22, 36]. Moreover, it was found that in 1 M HNO_3 solutions H_2O_2 formation is faster in ca. 2.4 times than in water at similar ultrasonic conditions. This striking phenomenon was explained by the scavenging of $OH^{\bullet}$ radicals with NO_3^- ions at the bubble/solution interface rather than by $OH^{\bullet}$ radicals recombination. The related mechanism described with the reactions (15-16) demonstrate that only one $OH^{\bullet}$ radical is necessary to form one H_2O_2 molecule whereas two are necessary in the reaction (6):

$$H_2O_2 + HNO_2 \rightarrow HNO_3 + H_2O \quad (14)$$
$$NO_3^- + H^+ + OH^{\bullet} \rightarrow NO_3^{\bullet} + H_2O \quad (15)$$
$$NO_3^{\bullet} + H_2O \rightarrow NO_2 + H_2O_2 \quad (16)$$

The formation of H_2O_2 in HNO_3 solutions has been demonstrated to be strongly influenced by the presence of oxygen [12]. At 20 kHz ultrasound, the yield of H_2O_2 in 1 M HNO_3 saturated with 20 vol.% O_2/Ar mixture is increased by about 2.3 times compared to pure water in agreement with the results obtained previously with Ar in HNO_3/$NaNO_3$ solutions [22]. On the other hand, at high-frequency ultrasound (207 and 615 kHz) the yield of H_2O_2 was found to be conversely higher in water than in 1 M HNO_3. It was concluded that the observed inhibition of H_2O_2 formation in HNO_3 solutions at high-frequency ultrasound is related to the higher yield of sonochemically formed NO_x when compared to 20 kHz ultrasound experiments. Formed NO_x gases thus enable the rapid oxidation of H_2O_2 even in the presence of anti-nitrous reagents.

3 Sonochemical reactions of actinides in homogeneous solutions

Table 1 summarizes the data dealing with redox reactions of actinide ions driven by power ultrasound in homogeneous aqueous solutions. Most of these studies have been performed in nitric acid solutions. In this medium, the redox reactions of actinides are driven by the formation of HNO_2 produced from nitric acid sonolysis or, in the presence of anti-nitrous reagents, by the formation of H_2O_2 originated from sonochemical water splitting.

Uranium. It was shown that at [HNO_3] = 0.1-1.0 M the oxidation of U(IV) to U(VI) is autocatalytic due to the sonochemical formation of HNO_2 and NO_2 oxidizing species [37]. Interestingly, U(IV) can be sonochemically oxidized in HNO_3 solutions even in the presence of hydrazinium nitrate, due to the in-situ generation of H_2O_2 [15]. This reaction follows zero-order kinetics. In HCl medium, U(IV) is oxidized to U(VI) at an appreciable rate only at the ultrasonic intensity higher than 3 $W \cdot cm^{-2}$ [37]. It was reported that in HNO_3 solutions the sonochemical reduction of U(VI) to U(IV) is possible in the presence of hydrazine, 2-PrOH and Pt black catalyst [38, 39]. On the other hand, Nikonov and Shilov have shown that in the presence of hydrazinium chloride U(VI) can be partially reduced to U(IV) under 44 kHz ultrasound at the ultrasonic intensity of about 10 $W \cdot cm^{-2}$ [37].

Neptunium. In contrast to U(IV), sonochemical oxidation of Np(V) to Np(VI) in 3 M HNO_3 is a reversible process [40]. Ultrasonic treatment leads to Np(V) oxidation in the first 30 min of the process. Np(V) oxidation then decelerated, and after approximately 1 h of sonication the formed Np(VI) was reduced back to Np(V). However, the addition of a small amount of urea ($2.5 \cdot 10^{-3}$ M) allowed to avoid Np(VI) reduction. These results were explained according to the equilibrium (17):

$$NpO_2^+ + 3/2\ H^+ + ½\ NO_3^- \rightleftharpoons NpO_2^{2+} + ½\ HNO_2 + ½\ H_2O \quad (17)$$

For short-time sonication, the concentration of generated HNO_2 is low and it plays the role of catalyst for Np(V) oxidation by nitrate ions. Long-time sonication causes HNO_2 to accumulate and it becomes a reducing agent for Np(VI) due to the close redox potentials observed for NO_3^-/HNO_2 (0.94 V/NHE) and Np(VI)/Np(V) (1.138 V/NHE). In the presence of anti-nitrous reagents, HNO_2 is scavenged, and Np(V) is found to be stable under ultrasound. Initially, hexavalent neptunium Np(VI) in 1 M HNO_3 and in the presence of 0.1 M NH_2SO_3H is reduced to Np(V) during sonication with 20 kHz ultrasound by the in situ formed H_2O_2 [41]. In 3 M HNO_3, Np(V) is slowly reduced to Np(IV) under sonication with 600 kHz ultrasound in the presence of 2-PrOH and $[N_2H_5][Cl]$ [39]. In 1 M HNO_3 or 1 M HCl, ultrasonic treatment causes slow oxidation of Np(IV) to Np(V), which was attributed to the reactions with sonolytic products of acids, such as HNO_2 or H_2O_2 respectively [42].

Table 1. Sonochemical reactions of actinides in homogeneous solutions.

Reaction	Sonicated medium	Ultrasonic conditions	Ref.
Uranium			
U(IV) → U(VI)	$[HNO_3]$ = 0.1-1.0 M	44 kHz, 1 W·cm^{-2}, Ar, 25 °C	[37]
U(IV) → U(VI)	[HCl] = 0.1-1.0 M	44 kHz, > 3 W·cm^{-2}, Ar, 25 °C	[37]
U(IV) → U(VI)	$[HNO_3]$ = 4.0 M $[N_2H_5][NO_3] = 5\cdot10^{-3}$ M	20 kHz, 1.8 W·cm^{-2}, Ar, 25 °C	[15]
U(VI) → U(IV)	$[HNO_3]$ = 1.0-3.0 M $[N_2H_5][Cl]$ 1 vol% 2-PrOH 20 vol%, Pt black	600 kHz, 3.1 W·cm^{-2}, Ar, 25 °C	[38, 39]
U(VI) → U(IV)	$[HNO_3$ (HCl)] = 0.1-1.0 M $[N_2H_5][Cl]$ 5 10^{-3} M	44 kHz, 10 W·cm^{-2}, Ar, 25 °C	[37]
Neptunium			
Np(V) ⇌ Np(VI)	$[HNO_3]$ = 3.0 M	20 kHz, 1 W·cm^{-2}, Ar, 25 °C	[40]
Np(VI) → Np(V)	$[HNO_3]$ = 1.0 M $[NH_2SO_3H]$ = 0.1 M	20 kHz, 1 W·cm^{-2}, Ar, 25 °C	[41]
Np(V) → Np(IV)	$[HNO_3]$ = 3.0 M $[N_2H_5][Cl]$ 1 vol% 2-PrOH 20 vol%	600 kHz, 3.1 W·cm^{-2}, Ar, 25 °C	[39]
Np(IV) → Np(V)	$[HNO_3$ (HCl)] = 1.0 M	44 kHz, 1 W·cm^{-2}, Ar, 25 °C	[42]
Plutonium			
Pu(IV) → Pu(III)	$[HNO_3$ (HCl)] = 1.0 M $[N_2H_5][Cl]$ 5 10^{-3} M	44 kHz, 1 W·cm^{-2}, Ar, 20 °C	[43]
Pu(IV) → Pu(III)	$[HNO_3]$ = 1.0 M $[N_2H_5][NO_3]$ = 0.1 M $[NH_2SO_3H]$ = 0.1 M	20 kHz, 0.26-0.45 W·mL^{-1} Ar, 25 °C	[36]
Pu(IV) → Pu(III)	$[HNO_3]$ = 1.0-3.0 M $[N_2H_5][Cl]$ 1 vol% 2-PrOH 20 vol%, Pt black	600 kHz, 3.1 W·cm^{-2}, Ar, 25 °C	[39]
Pu(VI) → Pu(V)	pH = 2.8-3.6	203 kHz (0.13 W·mL^{-1}), Ar/20%O_2 20 kHz (0.34 W·mL^{-1}), 20 °C	[44]
2Pu(V) → Pu(IV) + Pu(VI)	$[HNO_3]$ = 0.25-0.5 M $[H_2C_2O_4]$ = 0.05 M	22 kHz, 0.9 W·cm^{-2}, Ar, 20 °C	[45]
Americium			
Am(VI) → Am(V)	$[HNO_3$ (HCl)] = 0.5 M	44 kHz, 1 W·cm^{-2}, Ar, 25 °C	[46]

***Plutonium*.** Reduction of Pu(IV) to Pu(III) is an industrially important process. Several authors reported the significant acceleration of Pu(IV) reduction to Pu(III) by hydrazine in HNO_3 and HCl solutions under the effect of ultrasound [36, 39, 43]. Nikonov and Shilov reported ca. 10 times acceleration of Pu(IV) reduction by hydrazine under 44 kHz ultrasound, whereas ultrasound does not have a significant effect on the reaction with hydroxylamine [43]. Virot et al. investigated the Pu(IV) sonochemical reduction in

1 M HNO_3 in the presence of hydrazinium nitrate or sulfamic acid. The latter compound is known to be a strong anti-nitrous reagent but inefficient as a reducing reagent [36]. The reduction of Pu(IV) in this system has been attributed to the reaction with H_2O_2 accumulated in 1 M HNO_3 submitted to ultrasound in the presence of anti-nitrous reagent and to the reaction with Ti(III) formed during the cavitation erosion of the ultrasonic probe. In the absence of anti-nitrous reagents, Pu(III) is rapidly oxidized to Pu(IV) in 1 M HNO_3 under ultrasound [36, 43]. By contrast, Pu(IV) could be sonochemically reduced to Pu(III) in 1 M HCl solutions by the reaction with H_2O_2 [42]. In weakly acid solutions, Pu(VI) can be reduced quantitatively to Pu(V) under sonication in the presence of Ar/20%O_2 gas mixture [44]. The mechanism deals with the reduction by in situ generated H_2O_2. It was shown that the kinetics of this reaction is strongly influenced by ultrasonic frequency. At 200 kHz, the reduction of Pu(VI) is completed in ca. 2 h of ultrasonic treatment. By contrast, several days are required to reduce Pu(VI) at 20 kHz ultrasound, which is due to the much lower yield of H_2O_2 observed at low-frequency ultrasound. Figure 2 reveals a striking behavior of Pu(VI) concentration during sonication by 20 kHz ultrasound. First, Pu(VI) reduction continues overnight when sonication was stopped. Such observation has been explained by the overproduction of H_2O_2 during sonication indicating that the limiting stage is a reaction between Pu(VI) and H_2O_2 rather than sonochemical production of H_2O_2. Another striking observation was a short-term increase of Pu(VI) concentration when ultrasound is started again. It was suggested that this phenomenon is related to Pu(V) re-oxidation with $HO_2^{\bullet}$ radicals. More generally, this approach allowed the rapid and simple preparation of relatively stable Pu(V) solutions at the millimolar range, free from additional reagents and other oxidation states. Hence, the authors further probed the structural and magnetic properties of Pu(V) aqueous ion. Finally, it was reported that the observed rate constant of Pu(V) disproportionation is ca. 1.8 time larger under ultrasound than under silent conditions [45]. In addition, the kinetic isotope effect $^{242}Pu/^{239}Pu$ ($\alpha = 1.008$) has been observed in this reaction. In terms of plasma chemical model of cavitation [20], both phenomena could be attributed to the vibrational excitation of PuO_2^+ cation in the liquid shell surrounding cavitation bubble by collisions with "hot" particles produced by sonochemical plasma.

***Americium*.** To the best of our knowledge, only one paper deals with the sonochemical reactions of americium. Nikonov et al. have shown that in 0.5 M $HClO_4$ or HNO_3, Am(VI) is rapidly reduced to Am(V) under ultrasound by sonolytic products, such as H_2O_2 and HNO_2 [46]. On the other hand, ultrasound accelerates the oxidation of Am(V) to Am(VI) with ozone in 1 M HNO_3 [46]. It was suggested that the sonochemical splitting of O_3 molecule yields highly oxidizing O atoms enabling efficient Am(VI) formation.

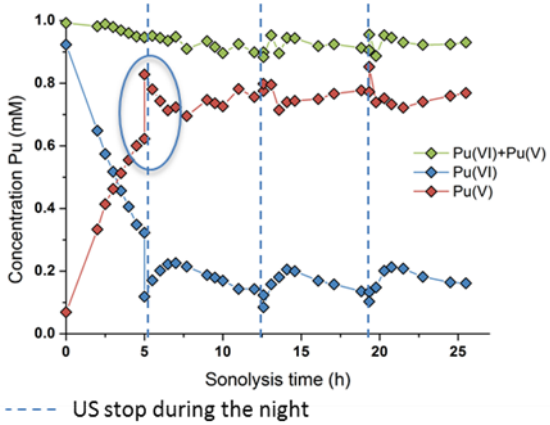

Figure 2: Behaviour of a 1 mM Pu(VI) solution under low frequency ultrasound (20 kHz, 0.34 W mL^{-1}, 21°C,Ar/(20%)O_2, pH = 3.5) as a function of sonolysis time. Reproduced from [44].

4 Sonochemical reactions of actinides in heterogeneous systems

Sonochemical reactions in solid/liquid systems attract a great deal of attention due to the unique combination of the chemical activity and mechanical effects of power ultrasound in heterogeneous media. At 20 kHz, the asymmetric collapses occurring at the vicinity of a solid boundary produce micro-jets with a maximal pressure of roughly 0.225 GPa [47-49]. On the other hand, quasi-spherical collapse at the distance smaller than twice the maximum bubble radius from the solid surface emits a shock wave with a peak pressure of several GPa at the solid boundary [50]. Both phenomena are responsible for the formation of microstreaming, microturbulence, micro-damage of solid surfaces, particle fragmentation, etc. [51]. These specific properties allow to consider power ultrasound as a useful tool for the enhancement of dissolution of refractory materials or for surface decontamination processes. It is worth noting that, unlike the chemical activity, the mechanical effects of power ultrasound are diminished when increasing the applied ultrasonic frequency, which is dealt with the decrease of a resonance bubble size.

Thorium. Potentially, thorium-based oxides can be used as nuclear fuel. However, ThO_2 is a highly refractory material towards dissolution. Therefore, the reprocessing of spent thorium fuel is one of the serious problems of the THOREX process [52]. Recently, the significant acceleration of the dissolution of ThO_2 in 5 M HNO_3 and 0.025 M HF mixtures was reported under the effect of 20 kHz ultrasound at room temperature [53]. This effect was attributed to the local heating produced by cavitation rather than to the fragmentation of ThO_2 particles. On the other hand, significant reduction of ThO_2 particle size was observed during ultrasonic treatment at 20 kHz in pure water [54]. It is important to emphasize that dissolution of ThO_2 is not observed when sonicated in pure water. In dilute 0.5 M H_2SO_4, sonication at 20 kHz under Ar/20% O_2 gas mixture causes the significant dissolution of ThO_2 nanoparticles at room temperature [55]. At high-frequency ultrasound (345 kHz) the acceleration of ThO_2 dissolution is not observed despite higher yields of H_2O_2, thus indicating the importance of the mechanical effects provided at low ultrasound frequency for an efficient dissolution. The suggested chemical effect leading to dissolution involves surface complexation of Th(IV) by H_2O_2 as it is illustrated in the Figure 3. Surprisingly, the extended ultrasonic treatment leads to the partial precipitation of a secondary phase composed of polymeric thorium peroxo sulfate, $Th(O_2)(SO_4)(H_2O)_2$ exhibiting a 1D morphology [56].

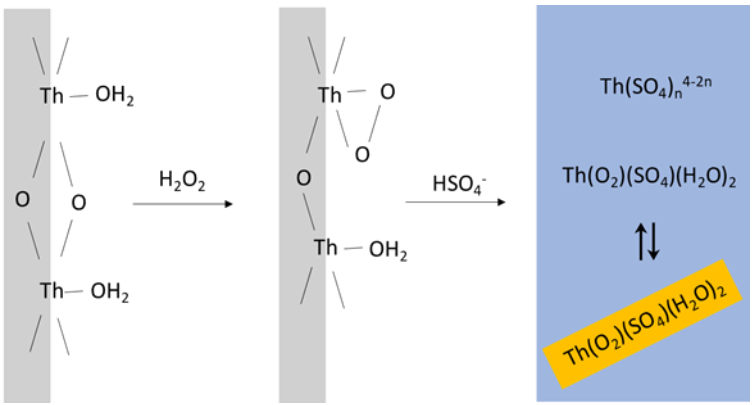

Figure 3: Suggested mechanism for ThO_2 dissolution and secondary phase formation. Reproduced from [46].

Uranium. Metallic uranium can be readily dissolved in mineral acids. However, the dissolution of U-Al-Si alloy, which is a principal component of some kinds of nuclear fuels, is passivated in nitric acid due to the formation of an aluminum oxide film at the surface. Ultrasonic treatment at 44 kHz significantly increases the rate of the alloy dissolution due to the particle size reduction and removal of Al_2O_3 film from the surface [57]. The oxidative dissolution of electrodeposited UO_2 films in aqueous H_2O_2 solutions was found to be accelerated under the effect of 40 kHz ultrasound [58]. The effect of the ultrasonic treatment was attributed to the removal of a studtite passivating layer from the surface of UO_2.

After dissolution, the re-precipitation of $UO_2O_2 \cdot 4H_2O$ does not occur due to the quite low concentration of uranium (< 1 mM). It was reported that the 20 kHz sonication of uranium carbide UC in 3 M HNO_3 reduces dramatically the induction period required for its dissolution due to the sonochemically generated HNO_2 [59]. However, a passivation re-appears after ca. 60% of dissolution, which was attributed to the accumulation of polymerized carbonaceous residues at the surface of UC. On the other hand, it was demonstrated that sonication provides a more effective total carbon removal during dissolution compared to silent conditions.

In the course of research activities dedicated to the study of new alternative techniques for the reprocessing of nuclear fuels while minimizing the generation of contaminated wastes, Samsonov et al. investigated the use of supercritical fluid carbon dioxide for the dissolution of actinide oxides [60]. Soluble complexes of U(VI) can be formed in supercritical fluid in the presence of complexing agents. While optimized conditions demonstrated the possible dissolution of UO_3 in supercritical CO_2 (150 atm, 600 °C) containing tri-butyl phosphate (TBP) and β-diketone thenoyltrifluoroacetylacetone (HTTA) with a final extraction efficiency of about 40%, the additional application of 44-48 kHz ultrasound during the extraction process allowed to recover 96.4% or uranium. This effect was suggested to result from the easiest removal of $UO_2(TTA)_2H_2O$ complexes formed at the solid surface under ultrasound irradiation [60, 61]. Similarly, Enokida et al. reported the dramatic increase of the dissolution kinetics of UO_2 powder in supercritical CO_2 in the presence of ultrasound [62]. The described system consisted in the sonication of two different cells of the experimental set-up: the first one consisting in the mixing of TBP extractant in aqueous HNO_3 media with supercritical fluid CO_2 whereas the second one consisting in the dissolution cell mixing UO_2 powder, glass beads and the extracting/supercritical CO_2 mixture arriving from the first cell. The Figure 4 illustrates the significant effect of the application of ultrasound on the dissolution of UO_2 in the described supercritical CO_2 system. Under ultrasound, the amount of uranium recovered yielded more than 73% after 20 min while the highest yield observed in silent conditions never exceeded 13%. The results were suggested to result from an increased mass transfer occurring under ultrasound [62].

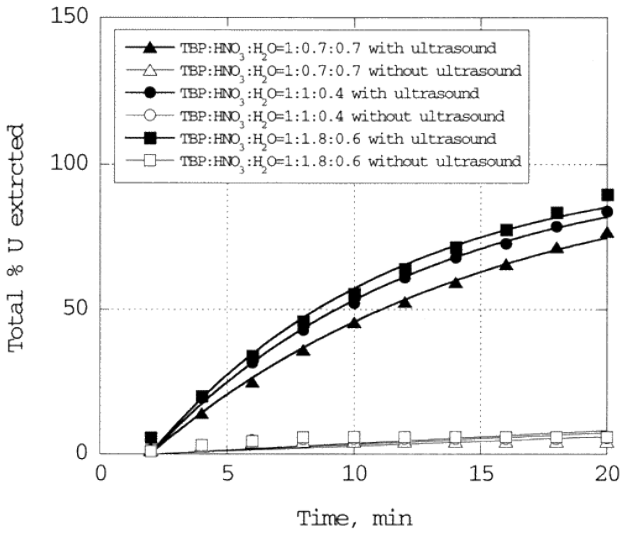

Figure 4: Dissolution kinetics observed for UO_2 in supercritical CO_2 containing TBP/HNO_3/H_2O mixture at 323 K and 15 MPa with and without the application of ultrasound. Reproduced from [62].

The removal of uranium from solid matrixes is an important process of solid radioactive wastes decontamination. In most cases, uranium recovery can be achieved by controlled dissolution. The magnesiothermic reduction of uranium fluoride UF_4 to prepare uranium metal as a nuclear fuel for some reactors generally requires calcium or magnesium generating metal MgF_2 or CaF_2 slag by-products containing 2-5% of uranium. Kalsi and coworkers investigated the recovery of U from MgF_2 slags (50 g) by sonicating 2-7.5 M HNO_3 solutions in an ultrasonic bath. The authors reported the significant

increase of the dissolution of uranium under ultrasound and under O_2 atmosphere [63]. Alternatively, the enhanced uranium leaching observed by Avvaru et al. during the 20 kHz ultrasound treatment of powdered MgF_2 in HNO_3 solutions stems from the increase of the surface diffusion coefficient and particle size reduction [64]. Kinetic studies have shown that this process is limited by pore diffusion resistance. Ultrasonically assisted recovery of uranium from silica nanoparticles, SiO_2, and its functionalized biohybrid, SiO_2-BH, loaded with UO_2^{2+} ions has been studied by Lahiri et al. [65]. They found that 20–40 kHz ultrasound accelerates in ca. 2-5 times uranium removal from SiO_2 and SiO_2-BH quasi spherical 12-17 nm nanoparticles in nitric acid solutions when compared to silent conditions. An activation energy of less than 20 $kJ \cdot mol^{-1}$ indicates the diffusion-controlled mechanism in the studied system. On the other hand, uranium leaching into 6-8 M HNO_3 solutions from uranium-impregnated spherical graphite tokens with a diameter of ca. 15 mm is accelerated on 7-15% only under the effect of 20-40 kHz ultrasound [66]. However, at $[HNO_3]$ = 12 M and 20 kHz ultrasound the significant loss of uranium is observed due to the graphite erosion and formation of graphitic dust.

Ultrasound-assisted removal of contaminants from the extended surfaces is probably the most known application of power ultrasound [67]. In comparison to civilian industries, publications dealing with ultrasonic cleaning in the nuclear sphere are very rare in the literature, but the technique nevertheless has still appeared of interest for particular applications. For instance, some reports describe the application of ultrasound for the radionuclide surface decontamination of fuel pins and assemblies [68-70]. A report from EPRI, USA hence describes full-scale ultrasonic tests on discharged nuclear assemblies in the spent fuel pool of Callaway plant (1999) [71]. Sixteen high-energy transducers operated at 25 kHz were used to remove crud deposition from Zr-fuel rods, which is known to possibly interfere with nuclear smooth operation (e.g., heat distribution, corrosion or failure of the rods). The report indicates that 70-80% of the corrosion products have been removed using this mild approach (5-10 min at approx. 30 °C) before reloading the assembly for re-irradiation [71]. A similar example can be found in the very interesting survey provided by Lebedev et al. about the application of the ultrasonic technologies in nuclear engineering [70]. In particular, the development of an ultrasonic system for the cleaning of rod fuel assemblies from WWER (Water Water Energy Reactor) reactors before service is described. More recently, Kumar et al. described the decontamination of full-scale fast reactor fuel pins installed on the production line. Decontamination was performed with 40 transducers operated at 38 kHz in water. Optimized conditions were observed at approx. 45°C and allowed to reach a decontamination efficiency higher than 99% [69]. More recently, ultrasound-assisted uranium removal from Mg and Mg-Zr alloy has been reported by Ji et al. [72]. Tubes fabricated from Mg-Zr alloy were a principal component of nuclear fuel cladding used in UNGG reactors that operated in France between 1956 and 1994. Today, contaminated Mg-based claddings constitute large volume of high-level solid wastes. One of the potential options for their management consists in their partial decontamination allowing further ground storage. Ji et al. demonstrated that sonication of genuine UNGG cladding materials and simulants at 345 kHz in 0.01 M oxalic acid solution provides a rapid and effective surface decontamination [72]. Figure 5 shows that a decontamination factor higher than DF = 100 can be reached after 20 minutes of ultrasonic treatment at room temperature. The mechanism of decontamination consists of the ultrasonically controlled surface dissolution of the Mg-based substrate, which has been found to be structured with homogeneous ca. 100 µm craters during treatment. The approach has been demonstrated to be particularly interesting when compared to conventional stirring (DF= 5 after 90 min for Mg/Zr simulant). Interestingly, a recontamination process of the surface was observed after treatment which phenomenon was attributed to the sorption of aqueous uranyl ions (initially removed from the sonicated surface) by $Mg(OH)_2$ secondary phase (brucite) neo-formed during treatment [72, 73].

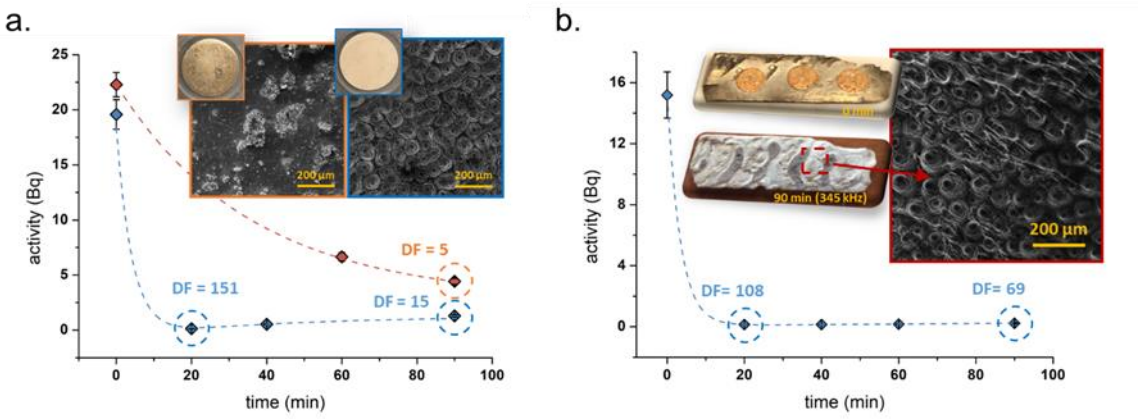

Figure 5: (a) Alpha-radioactivity evolution of U-contaminated Mg-Zr surfaces treated in 0.01 M oxalic acid under stirring (100 rpm) with (blue curve) and without (red curve) ultrasound. Inserts: Optical and SEM pictures of U-contaminated Mg-Zr surfaces. (b) Ultrasound-assisted decontamination of a fin UNGG fragment. Inserts show optical and SEM pictures of the sample before and after decontamination. Decontamination conditions: 345 kHz, 90 min, Ar, 20°C, 100 rpm, P_{ac}= 40 W. Reproduced from [72].

***Neptunium*.** Nikonov et al. reported that ultrasonic treatment at 44 kHz of NpO_2OH suspension in 1 M LiOH saturated with N_2O leads to the partial oxidation of Np(V) to Np(VII) [74]. In aerated or argon-saturated LiOH solution, the oxidation of Np(V) was not observed. The addition of persulfate ion also did not lead to Np(VII) formation. The mechanism of Np(VII) formation is not clear. One can suggest that the splitting of N_2O molecule inside the bubble causes formation of oxygen atom (E° = 2.42 V) that enables oxidizing Np(V) at the bubble/solution interface. It is interesting to note that only Np(VI) is formed in neutral N_2O-saturated aqueous solutions. Sonication of NpO_2 suspension in 1 M LiOH enhances the oxidation of Np(IV) to Np(VII) by ozone most likely also due to the atomic oxygen formation [75].

***Plutonium*.** The dissolution of metallic plutonium in nitric acid solutions was considered as one of the alternatives for the conversion of military-grade plutonium to MOX nuclear fuel [76]. However, Pu metal is known to dissolve very slowly in HNO_3 because of passivation. Nevertheless, it was reported that Pu and Pu/Ga alloys could be dissolved in HNO_3-HCOOH mixtures at room temperature [76]. However, a significant dissolution rate can be reached only at quite high concentrations of HNO_3 (ca. 3.5 M) and HCOOH (ca. 3 M) which also leads to non-controllable denitration occurring during dissolution at such conditions. It was reported that Pu metal dissolution can be considerably accelerated in more dilute solutions using power ultrasound [77]. At the ultrasonic frequency of 20 kHz and intensity 1 $W \cdot cm^{-2}$ in the presence of argon, the dissolution rate increases by ca. 17 times at [HNO_3] = 0.5 – 1.0 M and [HCOOH] = 1.0 – 2.0 M without undesirable denitration. Dissolution at such conditions is accompanied by Pu(III) accumulation in solution. It was assumed that cavitation removes the passivating layer from the metal surface and accelerates of the mass transfer at the liquid/solid interface.

The dissolution of refractory PuO_2 is an important step in the manufacturing of MOX fuel and high-level solid waste reprocessing as well. While classical conditions requires the use of concentrated mixtures of boiling or hot HNO_3 in the presence of HF or AgO, the effect of ultrasound on PuO_2dissolution has been demonstrated to be promising by several research groups. Nikonov and Shilov reported the significant acceleration of PuO_2 oxidative dissolution in 1 M LiOH with 44 kHz ultrasound in the presence of ozone [75]. Accumulation of Pu(VII) during dissolution indicated the effect of strong oxidizing species, probably, atomic oxygen as it was suggested for the system with NpO_2 at similar conditions [75]. It was shown that 20 kHz ultrasound has no effect on PuO_2 dissolution even in concentrated HNO_3 and the concentration of plutonium in solution after ultrasonic treatment does not exceed the calculated thermodynamic solubility of PuO_2 [78]. On the other hand, Juillet et al. reported

a different result with the ca. 3 and 4 times acceleration of PuO_2 dissolution in 4 M HNO_3 under the effect of 20 kHz and 500 kHz ultrasound respectively [79]. This discrepancy could be explained by the fact that the authors [78] used the ultrasonic bath reactor without direct contact of the ultrasound emitter with sonicated solution. In general, ultrasonic bath configuration provides a much lower absorbed acoustic power when compared to the ultrasonic horn directly immersed in the treated solution as it was used in the work [79]. Meanwhile, non-direct ultrasonic treatment at 20 kHz provides quantitative dissolution of PuO_2 in 8 M HNO_3-4 M HF mixture, which is unachievable under silent conditions at near room temperature [78]. At 20 kHz ultrasound, the rate of PuO_2 oxidative dissolution by AgO in HNO_3 solutions is at least twice than the one observed in silent conditions [78, 80]. On the other hand, high-frequency ultrasound (500 kHz) has no influence on the dissolution rate of PuO_2 indicating the importance of the mechanical effects provided by ultrasound which lead to a particle size reduction and an acceleration of the mass transfer [79]. The authors [78] noted that the efficiency of PuO_2 oxidative dissolution is decreased in the presence of river sediments because of parasitic consumption of Ag(II) by oxidizable components of sediments.

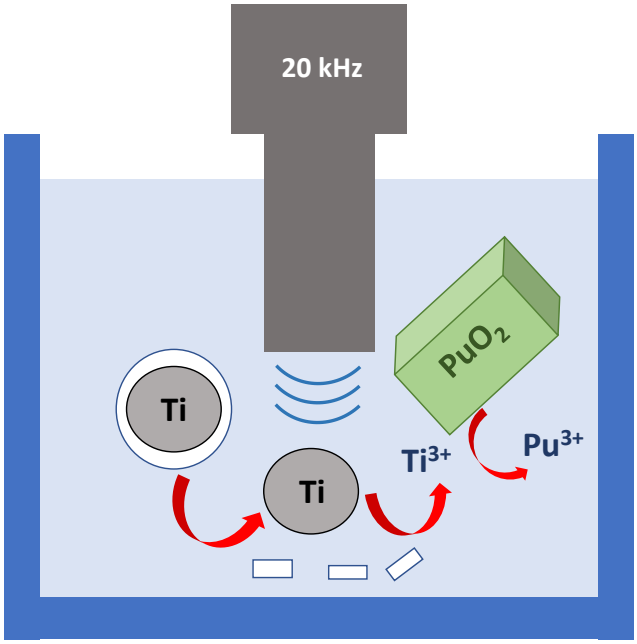

Figure 6: Graphical sketch of ultrasonically assisted reductive dissolution of PuO_2.

Reductive dissolution of PuO_2 can be performed under softer conditions than the one required for oxidative or complexing dissolution and can therefore be considered as an alternative to these processes. It was reported that the addition of $TiCl_3$ solution to the suspension of PuO_2 in sonicated (20 kHz) HNO_3 solution results in 40% dissolution due to Pu(IV) reduction to soluble Pu(III) species [78]. It should be noted that Ti(III) is unstable in the presence of nitrate-ions and rapidly oxidizes to TiO^{2+}, which decreases the efficiency of PuO_2 reductive dissolution. The application of ultrasound most likely enhances the diffusion of Ti(III) to the surface of PuO_2. On the other hand, formation of HNO_2 during sonolysis of HNO_3 would favor Ti(III) oxidation. The authors [80] studied the ultrasound-assisted reductive dissolution of PuO_2 (S_{BET} = 5 $m^2 \cdot g^{-1}$) in nitric acid medium in the presence of Ti metal microparticles (325 mesh). At [HNO_3] = 0.5 M, [$N_2H_5NO_3$] = 0.1 M and [HCOOH] = 2 M ultrasonic treatment at 20 kHz in the presence of Ar and at T = 33 °C caused the accumulation of Pu(III) in solution. It was concluded that ultrasound enables the depassivation of Ti surface followed by the production of

strongly reductive Ti(III) species. The principle steps of ultrasonically assisted reductive dissolution of PuO_2 are illustrated in Figure 6. The addition of hydrazine nitrate was required to remove HNO_2 formed by sonolysis of HNO_3. The experiments revealed the better efficiency of dissolution in the presence of HCOOH, which was attributed to the scavenging of oxidizing radicals formed during the sonochemical process. It should be noted that the injection of NH_4F up to 0.01M into the sonicated solution dramatically improves the reductive dissolution of PuO_2. At $[HNO_3]$ = 1.5 M, 42% of PuO_2 is dissolved in few minutes after NH_4F injection. However, after a short period of time, a low residual dissolution rate is finally observed. The accelerating effect of the fluoride ions was explained by the strong increase of Ti dissolution in the presence of fluoride. On the other hand, a steady-state of further dissolution was assigned to the passivation of PuO_2 surface. The origin of the passivation phenomenon is still not clear. It should be noted that the efficiency of the reductive dissolution is dependent upon PuO_2 specific surface area. For the sample of PuO_2 with S_{BET} = 14 $m^2 \cdot g^{-1}$ the ultrasound-assisted digestion of plutonium dioxide was complete [80].

5 Sonochemical synthesis of actinide nanoparticles

Nanochemistry of actinides is an emerging branch of actinide chemistry important for fundamental, environmental and material sciences [81]. Sonochemistry has been employed for the synthesis of nanomaterials since a long time [82]. However, for the preparation of actinide nanoparticles this technique started to be used relatively recently. It was reported that the ultrasonic irradiation of Th(IV), Np(IV) and Pu(IV) β-diketonates in hexadecane (f = 20-22 kHz, P_{ac} = 0.4 $W \cdot mL^{-1}$, Ar, T = 92-103 °C) causes their degradation forming nanometric-size solid products [83-85]. The rate of sonochemical process increases with the increase of metal β-diketonate volatility. It was found that the solid sonication products consisted of a mixture of actinide carbides and the partial degradation products of initial metal β-diketonates. The mechanism of sonolysis was interpreted in terms of a two-site model of the sonochemical processes: metal carbides are formed in a sonochemical plasma inside the cavitation bubble, and partial degradation products are formed at less drastic conditions of the liquid reaction zone surrounding the bubble. It is noteworthy that the heating of Th(IV) solid degradation products at 800 °C yields round-shaped nanoparticles of ThO_2 with the size in the range of 20-40 nm.

Ultrasound assistance has been reported to be effective during the synthesis of Ce, U and Th oxide nanoparticles embedded in a mesoporous matrix [86]. Sonication (35 kHz) was used to facilitate the entry of metal ions into the synthesized MCM-41 porous structures before the pH was adjusted and calcination occurred (250 °C, 2 h in air). While conventional stirring was found to be not efficient when embedding silica structures with pore diameters lower than 5 nm, ultrasound allowed to homogeneously distribute the Th(IV), Ce(IV) and U(VI) oxide nanoparticles within the mesoporous matrix. The ultrasound-assisted synthesis of thorium-based organic frameworks (Th-MOF) was recently described by Sargazi et al.[87]. The original approach consisted in combining the reverse-micelle method with an ultrasound irradiation. The nanostructures were obtained from a mixture composed of thorium (IV) nitrate pentahydrate and 2,6-pyridine dicarboxylic acid which were added to a solution containing sodium dodecyl sulfate and n-hexane (stirred at 85°C during 1 h) before being sonicated at 40 °C during 21 min. The Figure 7 illustrates the morphological differences observed for Th-MOF nanostructures prepared by the conventional or ultrasonic approaches, the latter yielding more uniform and non-aggregated particles of 27 nm. In comparison to the typical reverse-micelle procedure, the additional sonication of the system allowed the rapid nucleation of crystals and offered a better thermal stability, a higher specific surface area and smaller particle size for the as-synthesized MOF [87].

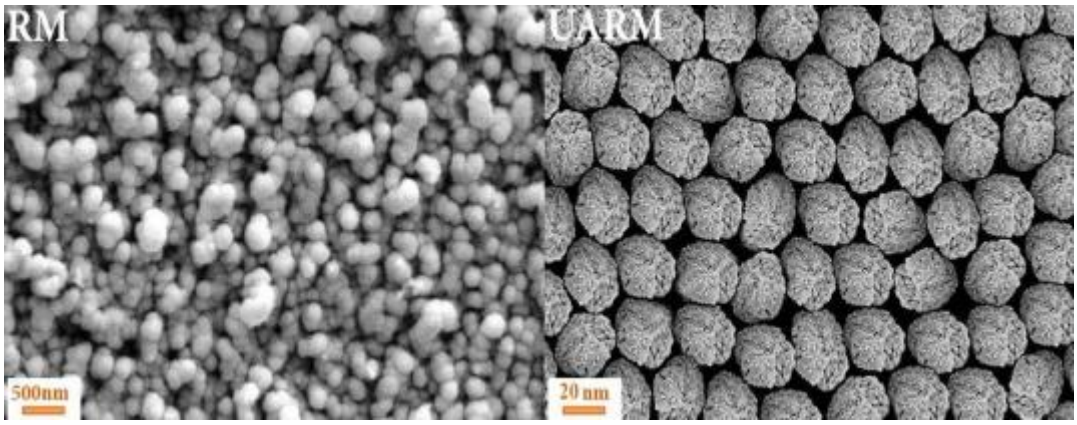

Figure 7: SEM images acquired on Th-MOF samples prepared by reverse micelle method without (RM) and with (UARM) additional ultrasound irradiation. Reproduced from [78].

Sonochemistry was shown to be effective for the preparation of actinide nanocolloids. Prolonged ultrasonic treatment of PuO_2 suspension in pure water with 20 kHz ultrasound produces a relatively stable salt-free plutonium colloid [88]. The efficiency of this surprising process strongly depends on experimental conditions. The yield of Pu colloid in the presence of 10 vol. %CO/Ar gas mixture is almost 3 times greater than that with pure Ar. In addition, the formation of Pu colloid is not observed in water saturated with Ar/O_2 mixture. The rate of Pu colloid formation increases with the increase of PuO_2 specific surface area. In agreement with this observation, the kinetic curves observed for Pu colloid formation display an induction period indicating that ultrasonic fragmentation of PuO_2 particles largely enhances colloid formation. Therefore, it was concluded that the sonochemical formation of Pu colloid results from the unique combination of mechanical and chemical effects of acoustic cavitation. As it was mentioned above (see the reactions 8-9), CO provides the reducing conditions during sonochemical treatment of water due to the scavenging of $OH^{\bullet}$ radicals. Consequently, it was assumed that the mechanism of the sonochemical Pu colloid formation includes Pu(IV) reduction at the surface of PuO_2 with hydrogen atoms produced by cavitation bubble, solubilization of Pu(III) species and their re-oxidation into Pu(IV) yielding colloid through hydrolysis processes. The approach provides a slow but continuous accumulation of colloids which might explain the absence of other Pu oxidation states in the sonochemical colloids. Indeed, conventional hydrolytic approaches most often show mixtures of Pu(IV) colloids with amounts of Pu(VI) as a result of a competition between disproportionation and hydrolysis reactions for Pu(IV). HRTEM images shown in Figure 8 reveal the particle size observed for the sonochemical Pu colloid (d= 7.1±1.2 nm) which is larger than that of Pu colloid obtained by hydrolysis of Pu (d= 2.9±0.4 nm). This observation is consistent with the contribution of the Pu(IV)-Pu(III)-Pu(IV) redox process into the overall mechanism since it is known that the autoxidation of Pu(III) in weakly acid solutions yields larger colloidal particles [89]. The electron diffraction patterns (Figure 8) point out the presence of PuO_2 particles with the *fcc* crystal structure for both sonochemical and hydrolytic Pu colloids. Further Pu L_{III}-edge X-ray absorption spectroscopy confirmed that both colloids are composed of PuO_2 nanocrystals [88, 90]. It was concluded that Pu(IV) intrinsic colloidal particles can be described as core-shell nanoparticles composed of PuO_2 core covered with a disordered Pu-O shell, which correlates with the particle size. Small-angle X-ray scattering studies revealed some morphological differences for hydrolytic and sonochemical Pu colloids: hydrolytic colloid was found to form spherical particles of ca. d= 4.0 nm which is close to HRTEM measurements whereas the sonochemical colloid showed elongated morphologies measuring 5.7 nm of thickness and >30 nm long, which was attributed to PuO_2 nanoparticles aggregation [91].

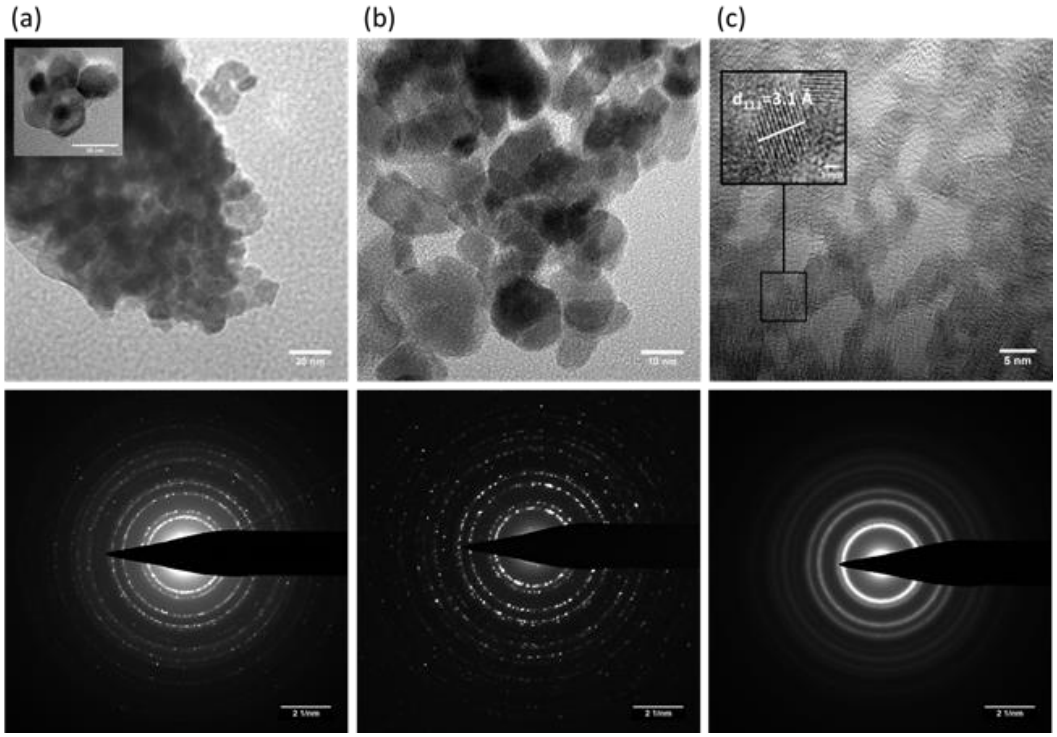

Figure 8: HRTEM images and electron diffraction patterns of studied Pu NPs. (a) nanostructured PuO_2 used for the preparation of the sonochemical Pu colloid, (b) sonochemical Pu colloid, (c) hydrolytic Pu colloid. Reproduced from [88].

Recently, it was reported that the sonication with 20 kHz ultrasound of A-UO_3 and β-UO_3 suspensions in pure water saturated with 10 vol. %CO/Ar gas mixture boosts the transformation of both forms of UO_3 into schoepite precipitates, $(UO_2)_4O(OH)_6 \cdot 6H_2O$, and stable uranium intrinsic colloids [92]. The addition of CO was required to avoid the formation of hydrogen peroxide during sonolysis of water. HRTEM, SAXS and U-L_{III} XAS studies allowed to conclude that the obtained uranium colloid is composed of quasi-spherical nanoparticles with the size of d= 3.8±0.3 nm and having a schoepite-like structure. The strong effect of ultrasound in the studied system was explained by the local heating of the liquid reaction zone of the cavitation bubble leading to the significant acceleration of UO_3 hydrolysis.

6 Some specific systems

In the literature, several sonochemical studies involving radionuclides have been reported, which are difficult to categorize. In 2009, Cardone et al. reported that the ultrasonic treatment at 20 kHz of very dilute aqueous solutions of ^{228}Th accelerates its radioactive decay by a factor 10^4 due to the "piezonuclear effect" based on the idea that the acoustic collapse generates extremely high local pressure in the vicinity of the bubble enabling influence of the radioactive decay [93]. However, several attempts to reproduce this effect have failed [94, 95]. In the work [94], the evolution of radioactivity for three isotopes of natural thorium (^{232}Th, ^{230}Th, ^{228}Th) during ultrasonic irradiation by 20 kHz power ultrasound was followed by α liquid scintillation counting technique. No change was detected in the α spectra even after several hours of treatment. It was concluded that the "piezonuclear effect" does not really exist in acoustic cavitation. In fact, the energy density of the shock waves created in water during multi-bubble cavitation at 20 kHz was estimated as ca. 5.5 $mJ \cdot mm^{-2}$ [48], which is about 8-times smaller than the energy density of laser-induced shock wave during enhanced breakdown emission spectroscopy. Obviously, this energy is not sufficient to accelerate the decay even of unstable nuclei.

Recently, Mason et al. reported the ultrasonically assisted dissolution of post-detonation nuclear debris using ammonium bifluoride (ABF) [96]. Post detonation nuclear debris examination requires the rapid dissolution of refractory minerals, including silicates, alumina, iron oxides and other minerals. It was shown that the sonication with 20 kHz ultrasound using cup horn system provides the rapid dissolution of these materials in the presence of ABF at less drastic conditions compared to conventional hydrothermal treatment with HF or ABF fusion technique. On the other hand, this study pointed out the difficulties with ultrasonic digestion of minerals based on TiO_2 and Al_2O_3 in acidic solutions. The mechanism of ultrasonic dissolution was attributed to the cavitation erosion of the solid surface and acceleration of the mass transfer.

In some cases, ultrasonic treatment allows to obtain new actinide compounds. For a long time, it was believed that uranyl aluminate could not be obtained from aqueous solutions due to the strong hydrolysis of UO_2^{2+} cations at pH > 6, where aluminate anions $Al(OH)_4^-$ become the dominating chemical form of dissolved aluminum. Nevertheless, it was found that ultrasonically assisted hydrolytic precipitation of U(VI) in the presence of mesoporous alumina MSU-X followed by thermal treatment at 800 °C yields ca. 5 nm uranyl aluminate (URAL) nanoparticles dispersed in the alumina matrix [97]. It is worth noting that the similar experiment under mechanical stirring leads mostly to U_3O_8 particles formation with only a small amount of URAL. Detailed EXAFS study pointed out that UO_2^{2+} cation in URAL is coordinated by bidentate aluminate groups AlO_2^- [97, 98]. In general, the yield of URAL nanoparticles depends on uranium concentration and calcination temperature. At 800 °C, URAL nanoparticles are formed only for a low uranium loading whereas at the content of uranium larger than 20 wt% U_3O_8 particles are formed with a size of ca. 20 nm. On the other hand, at 500 °C URAL nanoparticles are formed even for 25 wt% of uranium. A multistage mechanism of URAL formation has been suggested. At the first stage, ultrasonically assisted precipitation of ammonium diuranate provides highly dispersed uranium precursor at the surface of hydrated mesoporous alumina due to the strong mechanical effects provided by 20 kHz ultrasound. Further thermal treatment at 500 °C leads to U(VI) interaction with aluminate groups and formation of URAL. At the uranium loading higher than 2.5 wt%, heating up to 800 °C promotes the Ostwald ripening of URAL nanoparticles and their degradation to the thermodynamically more stable U_3O_8 species.

The remediation of soils polluted with heavy metals is a challenging topic from the environmental point of view. Anthropogenic activities significantly contributed in the dispersion and redistribution of radionuclides on the geosphere due to mining activities, accidents, space conquest or nuclear testing. The application of ultrasound for the decontamination of soils polluted with radionuclides has been investigated by several authors [99-101]. For instance, Radu et al. reported the ultrasonic treatment of soils artificially contaminated with uranium synthetic solutions showing a composition similar to what observed in mine residuals or dams [101]. In their study, a parametric study has been applied to find the optimized decontamination conditions in an alkaline extraction medium composed of NaCl and Na_2CO_3. Significant advantages were reported when sonicating the solids with an ultrasonic bath operated at 24 kHz and 50 °C at pH= 8. In particular, the decontamination yields increased by more than 25% while the required treatment duration decreased from 120 to 25 min when compared to mechanical stirring experiments. These results were explained by a combination of the local increase of the mass transfer and the fragmentation or erosion of the solid particle surfaces occurring under ultrasound irradiation [101].

Finally, several works focused on the ultrasonically assisted precipitation of uranium compounds. Doroshenko et al. obtained amorphous uranium solids containing phosphate groups by 20 kHz irradiation of UO_2X_2, where X is NO_3^-, CH_3COO^-, and acac (acetylacetonate) dissolved in organic extractants $OP(OR)_3$, where R is CH_3 and C_2H_5 [102]. This process allows removing ca. 30-35% of uranium during 8 h of treatment at 40 °C in argon. Phosphate required for uranium precipitation was produced in situ by sonochemical degradation of solvent. Calcination of the amorphous product at 1000 °C gives crystalline uranium phosphate UP_2O_7. Ultrasonic treatment at 35 kHz has been also shown to

accelerate the precipitation of ammonium uranyl tricarbonate $(NH_4)_4UO_2(CO_3)_3$ (AUC) from aqueous solutions compared to mechanical stirring [103]. In addition to enhanced kinetics, sonication improved the AUC crystallinity and reduced its particle size. The effect of ultrasound was attributed to the efficient nucleation due to the cavitation microbubbles and intensive acoustic microstreaming as well [103]. Khorshidi et al. applied 40 kHz ultrasound during the sample preparation step before spectrophotometric measurements were applied for the simultaneous determination of the concentrations of thorium and uranium in aqueous solutions [104]. The ultrasound-assisted emulsification micro-extraction approach consist in the rapid injection of small amounts of extracting solvents (carbon tetrachloride) in a sonicated aqueous media containing the elements of interest. The as-formed cloudy solution is then centrifuged to concentrate the solvent before micrometric volumes are taken with a syringe prior to analyses. The authors reported several advantages including an acceleration of the formation of fine cloudy solutions with a minimum consumption of organic solvent, a reduced extraction time and a better extraction efficiency [104].

Oktay and Yayli described the use of 35 kHz and 55 kHz ultrasound during the precipitation of thorium oxalate dihydrate [105]. In comparison to precipitates observed under conventional mechanical stirring, the authors reported similar cubic structures with a reduction of the particle size and distribution in addition to an increased specific surface area. Regarding the thermal conversion into oxides, the activation energies related to the decomposition of the precursors were found lower for the one obtained under ultrasound; in addition, the observation of a narrower temperature interval and a shorter period of time was noticed for their decomposition [105]. More recently, the precipitation of ammonium di-uranate (ADU) from uranyl nitrate with ammonia has been improved by the application of 35 kHz ultrasound irradiation [106]. ADU ($UO_3.xNH_3.(2-x)H_2O$) is an important intermediate in the preparation of UO_2 nuclear fuel and the quality of the latter highly depends on the operating parameters applied during the precipitation step for the former [107, 108]. Paik et al. demonstrated the dramatic increase of the precipitation kinetics when applying ultrasound on uranyl nitrate solutions (90 $g.L^{-1}$) in addition to the observation of a significant effect on the obtained powder properties. In comparison to a conventional stirring approach (400 rpm), the authors demonstrated a slightly better tap density (1.9 against 2.1 $g.cm^{-3}$, respectively) and higher specific surface area (10.4 against 28.7 $m^2.g^{-1}$, respectively) after ultrasound treatment. Also, XRD investigations revealed a higher crystallinity for the sonicated sample with a higher crystal size. Whatever the applied ultrasonic intensity or initial uranium concentration used during the precipitation step, the powders finally demonstrated smaller particle sizes with better distributions. The powder morphology is also significantly improved in agreement with the Figure 9. The final technological step consisting in the thermal conversion of ADU into UO_3 (550 °C, 4 h) also demonstrated a significant improvement in crystallinity with the observation of larger and more uniform agglomerates. These results were explained by the rapid diffusion of solutes under ultrasound due to the locally created better agitation and micro-mixing. The influence of the acoustic cavitation towards the formation of nuclei and the nucleation process via the decrease of the diffusion layer thickness was also mentioned [106].

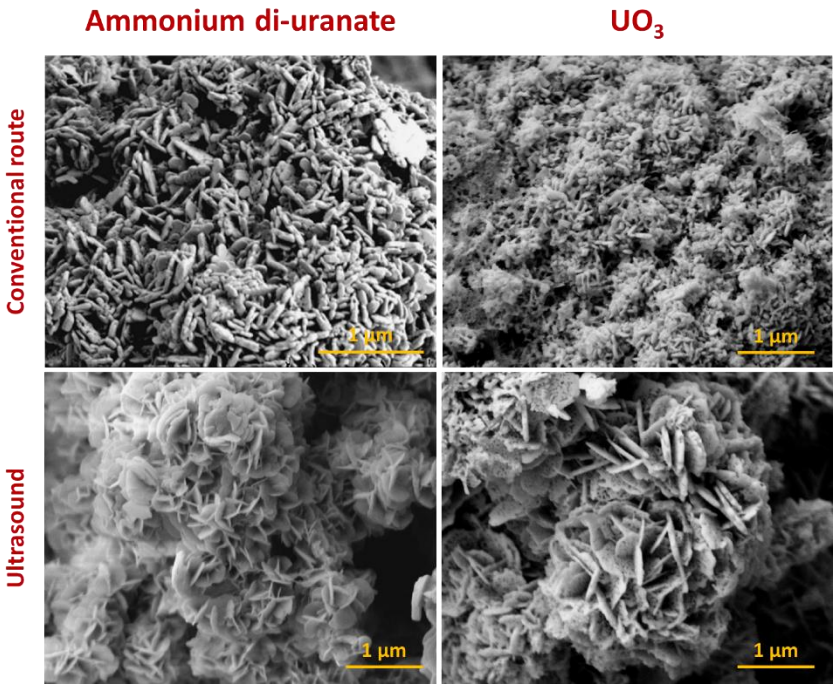

Figure 9: Selection of SEM pictures demonstrating the effect of 35 kHz ultrasound on the precipitation of ammonium di-uranate before and after calcination to prepare UO_3. Reproduced from [106].

7 Concluding remarks

In acidic aqueous solutions in the presence of Ar, sonochemical redox reactions of actinide ionic species are mostly driven by the secondary products of solvent sonolysis: H_2O_2 in water, HNO_2 in HNO_3, and HClO or Cl_2 in HCl solutions. However, in the presence of O_2 or O_3 the HO_2 radicals or O atoms respectively could also contribute. The efficiency of sonochemical reactions increases with the increase of ultrasonic frequency due to the higher yield of sonochemical products. In general, sonication promotes actinide oxidation. However, in the presence of $OH^{\bullet}$ radical scavengers, such as CO, the sonochemical reduction becomes efficient due to the release of H atoms and molecular hydrogen. In the future, it appears interesting to investigate the redox reactions of actinides in basic solutions where generation of solvated electrons in solutions is possible due to the H atoms conversion. It is worth noting that the hydrolysis of actinide ions in basic solutions also should be taken into account regarding the efficiency of sonochemical reactions.

In heterogeneous systems, both mechanical and chemical effects of power ultrasound are important. Further efforts will be addressed to understand and evaluate sonochemistry in solid-liquid systems in terms of refractory nuclear materials dissolution and preparation of actinide nanoparticles as well, which is very promising for future advanced nuclear systems. Ultrasound assisted precipitation is also a promising way to access actinide compounds with controlled particle size and morphology.

Finally yet importantly, ultrasonic decontamination is a domain of paramount interest since the global issue of dismantling of retired nuclear installations requires the development of new highly automatized technologies of radionuclide removal generating minimal volume of secondary harmful liquid wastes. Both low and high frequency ultrasound can result in significant benefits for industrial operations of decontamination of extended solid surfaces and dispersed materials as well, such as soils, mineral adsorbents and ion-exchange resins loaded with radionuclides.

Author contributions: All the authors have accepted responsibility for the entire content of this submitted manuscript and approved submission.

Research funding: None declared.

Conflict of interest statement: The authors declare no conflicts of interest regarding this article.

References

1. Richards W. T., Loomis A. L. The Chemical Effects of High Frequency Sound Waves I. A Preliminary Survey. *J. Am. Chem. Soc.* 1927, *49*, 3086-3100.
2. Schmitt F. O., Johnson C. H., Olson A. R. Oxidations Promoted by Ultrasonic Radiation. *J. Am. Chem. Soc.* 1929, *51*, 370-375.
3. Neppiras E. A. Acoustic cavitation. *Phys. Rep.* 1980, *61*, 159-251.
4. Fuchs F. J., 19 - Ultrasonic cleaning and washing of surfaces. In *Power Ultrasonics*, Gallego-Juárez, J. A.; Graff, K. F., Eds. Woodhead Publishing: Oxford, 2015; pp 577-609.
5. Chemat F., *Eco-extraction du végétal, procédés innovants et solvants alternatifs*. Dunod: 2015; p XI-322.
6. Ashokkumar M., Sunartio D., Kentish S., Mawson R., Simons L., Vilkhu K., Versteeg C. Modification of food ingredients by ultrasound to improve functionality: A preliminary study on a model system. *Innovative Food Science & Emerging Technologies* 2008, *9*, 155-160.
7. Feng H., Barbosa-Canovas G., Weiss J., *Ultrasound Technologies for Food and Bioprocessing*. Springer, New York, NY: 2011.
8. Adewuyi Y. G. Sonochemistry: Environmental science and engineering applications. *Industrial & Engineering Chemistry Research* 2001, *40*, 4681-4715.
9. Mahamuni N. N., Adewuyi Y. G. Advanced oxidation processes (AOPs) involving ultrasound for waste water treatment: A review with emphasis on cost estimation. *Ultrason. Sonochem.* 2010, *17*, 990-1003.
10. Bang J. H., Suslick K. S. Applications of Ultrasound to the Synthesis of Nanostructured Materials. *Adv. Mater.* 2010, *22*, 1039-1059.
11. Nikonov M. V. Chemical reactions of actinides under the effect of ultrasound, PhD thesis. Moscow, 1991.
12. Dalodière E., Virot M., Moisy P., Nikitenko S. I. Effect of ultrasonic frequency on H_2O_2 sonochemical formation rate in aqueous nitric acid solutions in the presence of oxygen. *Ultrason. Sonochem.* 2016, *29*, 198-204.
13. Humblot A., Grimaud L., Allavena A., Amaniampong P. N., De Oliveira Vigier K., Chave T., Streiff S., Jérôme F. Conversion of Ammonia to Hydrazine Induced by High-Frequency Ultrasound. *Angew. Chem. Int. Ed.* 2021, *60*, 25230-25234.
14. Mason T. J., Lorimer J. P., *Applied Sonochemistry, The uses of Power Ultrasound in Chemistry and Processing*. Wiley-VCH: Weinheim, 2002.
15. Venault L. De l'Influence des Ultrasons sur la Reactivité de l'Uranium (U(IV)/U(VI)) et du Plutonium (Pu(III)/Pu(IV)) en Solution Aqueuse Nitrique, PhD thesis. Paris XI, Orsay, France, 1998.
16. Juillet F. Etude de la dissolution d'oxydes réfractaires (CeO_2 et PuO_2) assistée par sonochimie, PhD thesis. Paris XI, 1997.
17. Nikitenko S. I., Venault L., Pflieger R., Chave T., Bisel I., Moisy P. Potential applications of sonochemistry in spent nuclear fuel reprocessing: A short review. *Ultrason. Sonochem.* 2010, *17*, 1033-1040.
18. Rubio F., Blandford E. D., Bond L. J. Survey of advanced nuclear technologies for potential applications of sonoprocessing. *Ultrasonics* 2016, *71*, 211-222.
19. Suslick K. S., McNamara W. B., Didenko Y. In *Hot spot conditions during multi-bubble cavitation*, NATO Advanced Study Institute on Sonochemistry and Sonoluminescence, Leavenworth, Wa, Aug 18-29, 1997; Leavenworth, Wa, 1997; pp 191-204.

20. Nikitenko S. I., Pflieger R. Toward a new paradigm for sonochemistry: Short review on nonequilibrium plasma observations by means of MBSL spectroscopy in aqueous solutions. *Ultrason. Sonochem.* 2017, *35*, 623-630.
21. Mark G., Tauber A., Rudiger L. A., Schuchmann H. P., Schulz D., Mues A., von Sonntag C. OH-radical formation by ultrasound in aqueous solution - Part II: Terephthalate and Fricke dosimetry and the influence of various conditions on the sonolytic yield. *Ultrason. Sonochem.* 1998, *5*, 41-52.
22. Nikitenko S. I., Venault L., Moisy P. Scavenging of OH radicals produced from H_2O sonolysis with nitrate ions. *Ultrason. Sonochem.* 2004, *11*, 139-142.
23. Petrier C., Jeunet A., Luche J. L., Reverdy G. Unexpected frequency effects on the rate of oxidative processes induced by ultrasound. *J. Am. Chem. Soc.* 1992, *114*, 3148-3150.
24. Ji R., Pflieger R., Virot M., Nikitenko S. I. Multibubble Sonochemistry and Sonoluminescence at 100 kHz: The Missing Link between Low- and High-Frequency Ultrasound. *J. Phys. Chem. B* 2018, *122*, 6989-6994.
25. Pflieger R., Chave T., Vite G., Jouve L., Nikitenko S. I. Effect of operational conditions on sonoluminescence and kinetics of H_2O_2 formation during the sonolysis of water in the presence of Ar/O_2 gas mixture. *Ultrason. Sonochem.* 2015, *26*, 169-175.
26. Margulis I. M., Margulis M. A. Dependence of the rate of formation of nitrate ions in water on the intensity and frequency of ultrasound waves. *Russian Journal of Physical Chemistry A* 2009, *83*, 2233-2237.
27. Misik V., Riesz P. In *Detection of primary free radical species in aqueous sonochemistry by EPR spectroscopy*, NATO Advanced Study Institute on Sonochemistry and Sonoluminescence, Leavenworth, Wa, Aug 18-29, 1997; Leavenworth, Wa, 1997; pp 225-236.
28. Okitsu K., Itano Y. Formation of NO_2^- and NO_3^- in the sonolysis of water: Temperature- and pressure-dependent reactions in collapsing air bubbles. *Chem. Eng. J.* 2022, *427*, 131517.
29. Supeno, Kruus P. Sonochemical formation of nitrate and nitrite in water. *Ultrason. Sonochem.* 2000, *7*, 109-113.
30. Ouerhani T., Pflieger R., Ben Messaoud W., Nikitenko S. I. Spectroscopy of Sonoluminescence and Sonochemistry in Water Saturated with N_2-Ar Mixtures. *J. Phys. Chem. B* 2015, *119*, 15885-15891.
31. Nikitenko S. I., Seliverstov A. F. A synergetic effect in nitrous acid formation by sonolysis of nitric acid in the presence of nitrous oxide. *Russ. Chem. Bull.* 2000, *49*, 2077-2079.
32. Hart E. J., Henglein A. Sonolytic decomposition of nitrous oxide in aqueous solution. *J. Phys. Chem.* 1986, *90*, 5992-5995.
33. Nikitenko S. T., Martinez P., Chave T., Billy I. Sonochemical Disproportionation of Carbon Monoxide in Water: Evidence for Treanor Effect during Multibubble Cavitation. *Angew. Chem. Int. Ed.* 2009, *48*, 9529-9532.
34. Venault L., Moisy P., Nikitenko S. I., Madic C. Kinetics of nitrous acid formation in nitric acid solutions under the effect of power ultrasound. *Ultrason. Sonochem.* 1997, *4*, 195-204.
35. Moisy P., Bisel I., Genvo F., Rey-Gaurez F., Venault L., Blanc P. Preliminary results on the effect of power ultrasound on nitrogen oxide and dioxide atmosphere in nitric acid solutions. *Ultrason. Sonochem.* 2001, *8*, 175-181.
36. Virot M., Venault L., Moisy P., Nikitenko S. I. Sonochemical redox reactions of Pu(III) and Pu(IV) in aqueous nitric solutions. *Dalton Trans.* 2015, *44*, 2567-2574.
37. Nikonov M. V., Shilov V. P. Redox reactions of uranium and plutonium under the effect of ultrasound. *Radiochimiya* 1990, *32*, 480-483.
38. Toraishi T., Kimura T., Arisaka M. A remote valency control technique: catalytic reduction of uranium(vi) to uranium(iv) by external ultrasound irradiation. *Chem. Commun.* 2007, 240-241.
39. Toraishi T., Kimura T., Arisaka M. Toward innovative actinide separation processes: Sequential reduction scheme of uranium, neptunium, and plutonium in 3 M HNO3 by external ultrasound irradiation. *J Nucl Sci Technol* 2007, *44*, 1220-1226.
40. Nikitenko S. I., Moisy P., Madic C. Sonochemical oxidation of Np(V) in aqueous nitric acid medium and sonochemical extraction of Np in two-phase TBP (30 vol.%)-n-dodecane/HNO3/H2O system. *Radiochim. Acta* 1999, *86*, 23-31.

41. Venault L., Moisy P., Nikitenko S. I., Madic C. In *Some sonochemical reactions of Np(IV) and Pu(IV) in acidic media* 11th Meeting of the European Society of Sonochemistry, La Grande Motte, France, June, 1-5th, La Grande Motte, France.
42. Nikonov M. V., Shilov V. P. Certain sonochemical reactions of Np(IV) and Pu(IV) in acidic media. *Sov. Radiochem.* 1990, *32*, 600-601.
43. Nikonov M. V., Shilov V. P. Effect of ultrasound on reduction of Pu(IV) by hydrazine and hydroxylamine in nitric and hydrochloric acids. *Sov. Radiochem.* 1989, *31*, 548-551.
44. Dalodière E., Virot M., Dumas T., Guillaumont D., Illy M. C., Berthon C., Guerin L., Rossberg A., Venault L., Moisy P., Nikitenko S. I. Structural and magnetic susceptibility characterization of Pu(V) aqua ion using sonochemistry as a facile synthesis method. *Inorg. Chem. Front.* 2018, *5*, 100-111.
45. Nikitenko S. I., Nikonov M. V., Garnov A. Y. Kinetics and kinetic isotope effect in pentavalent plutonium disproportionation activated by power ultrasound. *Journal of Radioanalytical and Nuclear Chemistry-Articles* 1995, *191*, 361-367.
46. Nikonov M. V., Shilov V. P., Krot N. N. Effect of ultrasound on redox reactions of americium in aqueous solutions. *Sov. Radiochem.* 1989, *31*, 545-548.
47. Dular M., Osterman A. Pit clustering in cavitation erosion. *Wear* 2008, *265*, 811-820.
48. Virot M., Chave T., Nikitenko S. I., Shchukin D. G., Zemb T., Mohwald H. Acoustic Cavitation at the Water-Glass Interface. *J. Phys. Chem. C* 2010, *114*, 13083-13091.
49. Virot M., Pflieger R., Skorb E. V., Ravaux J., Zemb T., Mohwald H. Crystalline Silicon under Acoustic Cavitation: From Mechanoluminescence to Amorphization. *J. Phys. Chem. C* 2012, *116*, 15493-15499.
50. Pecha R., Gompf B. Microimplosions: Cavitation collapse and shock wave emission on a nanosecond time scale. *Phys. Rev. Lett.* 2000, *84*, 1328-1330.
51. Franc J. P., Michel J. M., *Fundamentals of Cavitation*. Springer, Dordrecht, 2005; p XXII, 306.
52. Anantharaman K., Shivakumar V., Saha D. Utilisation of thorium in reactors. *J. Nucl. Mater.* 2008, *383*, 119-121.
53. Simonnet M. Thorium oxide dissolution : kinetics and mechanism

Dissolution de l'oxyde de thorium : cinétique et mécanisme. Université Paris Sud - Paris XI, 2015.
54. Morosini V., Chave T., Virot M., Moisy P., Nikitenko S. I. Sonochemical water splitting in the presence of powdered metal oxides. *Ultrason. Sonochem.* 2016, *29*, 512-516.
55. Bonato L., Virot M., Le Goff X., Moisy P., Nikitenko S. I. Sonochemical dissolution of nanoscale ThO_2 and partial conversion into a thorium peroxo sulfate. *Ultrason. Sonochem.* 2020, *69*, 105235.
56. Bonato L., Virot M., Dumas T., Mesbah A., Lecante P., Prieur D., Le Goff X., Hennig C., Dacheux N., Moisy P., Nikitenko S. I. Deciphering the Crystal Structure of a Scarce 1D Polymeric Thorium Peroxo Sulfate. *Chem. Eur. J.* 2019, *25*, 9580-9585.
57. Nikonov M. V., Panfilova S. E., Shilov V. P., Shirokova I. B. Effect of ultrasonic treatment on dissolution of nuclear fuel based on U-Al-Si alloy. *Radiochemistry* 1998, *40*, 230-231.
58. Nguyen T. V., Nguyen T. P. H., Le H. C. The effects of hydrogen peroxide solution and ultrasound on the dissolution of electrodeposited uranium oxide. *J Radioanal Nucl Ch* 2019, *319*, 1321-1329.
59. Virot M., Szenknect S., Chave T., Dacheux N., Moisy P., Nikitenko S. I. Uranium carbide dissolution in nitric solution: Sonication vs. Silent conditions. *J. Nucl. Mater.* 2013, *441*, 421-430.
60. Samsonov M. D., Trofimov T. I., Vinokurov S. E., Lee S. C., Myasoedov B. F., Wai C. M. Dissolution of Actinide Oxides in Supercritical Fluid Carbon Dioxide, Containing Various Organic Ligands. *J Nucl Sci Technol* 2002, *39*, 263-266.
61. Trofimov T. I., Samsonov M. D., Lee S. C., Smart N. G., Wai C. M. Ultrasound enhancement of dissolution kinetics of uranium oxides in supercritical carbon dioxide. *Journal of Chemical Technology & Biotechnology* 2001, *76*, 1223-1226.
62. Enokida Y., El-Fatah S. A., Wai C. M. Ultrasound-enhanced dissolution of UO_2 in supercritical CO_2 containing a CO_2-philic complexant of tri-n-butylphosphate and nitric acid. *Industrial & Engineering Chemistry Research* 2002, *41*, 2282-2286.

63. Kalsi P. K., Tomar B. S., Ramakumar K. L., Venugopal V. Studies on recovery of uranium from fluoride matrix employing sonochemistry. *J Radioanal Nucl Ch* 2012, *293*, 863-867.
64. Avvaru B., Roy S. B., Chowdhury S., Hareendran K. N., Pandit A. B. Enhancement of the leaching rate of uranium in the presence of ultrasound. *Industrial & Engineering Chemistry Research* 2006, *45*, 7639-7648.
65. Lahiri S., Bhardwaj R. L., Mandal D., Gogate P. R. Intensified dissolution of uranium from graphite substrate using ultrasound. *Ultrason. Sonochem.* 2020, *65*.
66. Lahiri S., Mishra A., Mandal D., Bhardwaj R. L., Gogate P. R. Sonochemical recovery of uranium from nanosilica-based sorbent and its biohybrid. *Ultrason. Sonochem.* 2021, *76*.
67. Mason T. J. Ultrasonic cleaning: An historical perspective. *Ultrason. Sonochem.* 2016, *29*, 519-523.
68. Kondoh K., Fujita C., Sakai H. *Ultrasonic cleaning of fuel assemblies*; United States, 1994; pp Medium: X; Size: pp. 787-791.
69. Kumar A., Bhatt R. B., Behere P. G., Afzal M. Ultrasonic decontamination of prototype fast breeder reactor fuel pins. *Ultrasonics* 2014, *54*, 1052-1056.
70. Lebedev O., Lebedev N., Gavrilov Y., Doilnitsyn V., Akatov A. In *Development and application of the ultrasonic technologies in nuclear engineering*, Scientific proceedings III International scientific-Technical conference "Innovations", Paris, France, 2017; Paris, France, 2017; pp 128-132.
71. Moser T., Carr T. *Pressurized Water Reactor Fuel Cleaning Using Advanced Ultrasonics, EPRI, Palo. Alto, CA, and AmerenUE, Fulton, MO: 2000. 1001052.*; 2000.
72. Ji R., Virot M., Pflieger R., Nikitenko S. I. Sonochemical decontamination of magnesium and magnesium-zirconium alloys in mild conditions. *J. Hazard. Mater.* 2021, *406*.
73. Ji R., Virot M., Pflieger R., Podor R., Le Goff X., Nikitenko S. I. Controlled "golf ball shape" structuring of Mg surface under acoustic cavitation. *Ultrason. Sonochem.* 2018, *40*, 30-40.
74. Nikonov M. V., Kuranov K. V., Shilov V. P. Sonochemical method for the preparation of neptunium(VII). *Bulletin of the Academy of Sciences of the Ussr Division of Chemical Science* 1988, *37*, 615-615.
75. Nikonov M. V., Shilov V. P. Sonochemical dissolution of NpO_2 and PuO_2 in aqueous basic media. *Sov. Radiochem.* 1990, *32*, 602-602.
76. Polyakov A. S., Zakharkin B. S., Rorisov L. M., Kucherenko V. S., Revjakin V. V., Bourges J., Boesch A., Capelle P., Bercegol H., Brossard P., Bros P., Sicard B., Bernard H., *Aida/MOX: progress report on the research concerning the aqueous processes for allied plutonium conversion to PuO_2 or $(UPu)O_2$*. Edition ANS: France, 1995.
77. Moisy P., Nikitenko S. I., Venault L., Madic C. Sonochemical dissolution of metallic plutonium in a mixture of nitric and formic acid. *Radiochim. Acta* 1996, *75*, 219-225.
78. Sinkov S. I. L., G. *Sonochemical Digestion of High-Fired Plutonium Dioxide Samples PNNL-16035,* ; 2006.
79. Juillet F., Adnet J. M., Gasgnier M. Ultrasound effects on the dissolution of refractory oxides (CeO2 and PuO2) in nitric acid. *J Radioanal Nucl Ch* 1997, *224*, 137-143.
80. Beaudoux X., Virot M., Chave T., Leturcq G., Jouan G., Venault L., Moisy P., Nikitenko S. I. Ultrasound-assisted reductive dissolution of CeO_2 and PuO_2 in the presence of Ti particles. *Dalton Trans.* 2016, *45*, 8802-8815.
81. Kalmykov S. N., Denecke M. A., *Actinide Nanoparticle Research*. 1st ed. 2011. ed.; Springer Berlin Heidelberg : Imprint: Springer: Berlin, Heidelberg, 2011.
82. Xu H., Zeiger B. W., Suslick K. S. Sonochemical synthesis of nanomaterials. *Chem. Soc. Rev.* 2013, *42*, 2555-2567.
83. Nikitenko S. I., Moisy P., Blanc P., Madic C. Sonolysis of actinide(IV) beta-diketonates in alkanes. *Comptes Rendus Chimie* 2004, *7*, 1191-1199.
84. Nikitenko S. I., Moisy P., Seliverstov A. F., Blanc P., Madic C. Sonolysis of metal beta-diketonates in alkanes. *Ultrason. Sonochem.* 2003, *10*, 95-102.

85. Nikitenko S. I., Moisy P., Tcharushnikova I. A., Blanc P., Madic C. Volatile metal beta-diketonates - new precursors for the sonochemical synthesis of nanosized materials - sonolysis of thorium(IV) beta-diketonates. *Ultrason. Sonochem.* 2000, *7*, 177-182.
86. Batuk O. N., Szabo D. V., Denecke M. A., Vitova T., Kalmykov S. N. Synthesis and characterization of thorium, uranium and cerium oxide nanoparticles. *Radiochim. Acta* 2013, *101*, 233-239.
87. Sargazi G., Afzali D., Mostafavi A. A novel synthesis of a new thorium (IV) metal organic framework nanostructure with well controllable procedure through ultrasound assisted reverse micelle method. *Ultrason. Sonochem.* 2018, *41*, 234-251.
88. Dalodiere E., Virot M., Morosini V., Chave T., Dumas T., Hennig C., Wiss T., Blanco O. D., Shuh D. K., Tyliszcak T., Venault L., Moisy P., Nikitenko S. I. Insights into the sonochemical synthesis and properties of salt-free intrinsic plutonium colloids. *Sci. Rep.* 2017, *7*.
89. Triay I. R., Hobart D. E., Mitchell A. J., Newton T. W., Ott M. A., Palmer P. D., Rundberg R. S., Thompson J. L. Size determinations of plutonium colloids using autocorrelation photon spectroscopy. *Radiochim. Acta* 1991, *52-3*, 127-131.
90. Bonato L., Virot M., Dumas T., Mesbah A., Dalodiere E., Blanco O. D., Wiss T., Le Goff X., Odorico M., Prieur D., Rossberg A., Venault L., Dacheux N., Moisy P., Nikitenko S. I. Probing the local structure of nanoscale actinide oxides: a comparison between PuO_2 and ThO_2 nanoparticles rules out PuO_{2+x} hypothesis. *Nanoscale Advances* 2020, *2*, 214-224.
91. Micheau C., Virot M., Dourdain S., Dumas T., Menut D., Solari P. L., Venault L., Diat O., Moisy P., Nikitenko S. I. Relevance of formation conditions to the size, morphology and local structure of intrinsic plutonium colloids. *Environmental Science-Nano* 2020, *7*, 2252-2266.
92. Cot-Auriol M., Virot M., Micheau C., Dumas T., Le Goff X., Den Auwer C., Diat O., Moisy P., Nikitenko S. I. Ultrasonically assisted conversion of uranium trioxide into uranium(vi) intrinsic colloids. *Dalton Trans.* 2021, *50*, 11498-11511.
93. Cardone F., Mignani R., Petrucci A. Piezonuclear decay of thorium. *Phys. Lett. A* 2009, *373*, 1956-1958.
94. Aupiais J., Cousin V., Nikitenko S. I., Pflieger R., Moisy P. Absence of Th-232,Th-230,Th-228 enhancement decay by ultrasound exposure. *Radiochim. Acta* 2013, *101*, 279-283.
95. Ford R., Gerbier-Violleau M., Vazquez-Jauregui E. Measurement of the thorium-228 activity in solutions cavitated by ultrasonic sound. *Phys. Lett. A* 2010, *374*, 701-703.
96. Mason C. A., Hubley N. T., Robertson J. D., Wegge D. L., Brockman J. D. Sonication assisted dissolution of post-detonation nuclear debris using ammonium bifluoride. *Radiochim. Acta* 2017, *105*, 1059-1070.
97. Chave T., Le Goff X., Scheinost A. C., Nikitenko S. I. Insights into the structure and thermal stability of uranyl aluminate nanoparticles. *New J. Chem.* 2017, *41*, 1160-1167.
98. Chave T., Nikitenko S. I., Scheinost A. C., Berthon C., Arab-Chapelet B., Moisy P. First Synthesis of Uranyl Aluminate Nanoparticles. *Inorg. Chem.* 2010, *49*, 6381-6383.
99. Panturu E., Jinescu G., Radulescu R., Olteanu A. F., Jinescu C. The Chemical Decontamination Process Intensification, using Ultrasounds. *Rev. Chim.* 2008, *59*, 1036-1040.
100. Radu A. D., Woinaroschy A., Panturu E. Uranium Extraction in Ultrasound Field from Contaminated Soils. *Rev. Chim.* 2014, *65*, 470-474.
101. Radu D. A., Isopescu R., Panturu E., Woinaroschy A. Optimization of uranium soil decontamination in alkaline washing using mechanical stirring and ultrasound field. *Environmental Science and Pollution Research* 2020, *27*, 5941-5950.
102. Doroshenko I., Zurkova J., Moravec Z., Bezdicka P., Pinkas J. Sonochemical precipitation of amorphous uranium phosphates from trialkyl phosphate solutions and their thermal conversion to UP2O7. *Ultrason. Sonochem.* 2015, *26*, 157-162.
103. Paik S., Satpati S. K., Gupta S. K., Sahu M. L., Singh D. K. Study on the effects of sonication on reactive precipitation of ammonium uranyl carbonate from pure uranyl nitrate solution. *J. Nucl. Mater.* 2021, *557*.

104. Khorshidi N., Niazi A. Moving window partial least squares after orthogonal signal correction as a coupling method for determination of uranium and thorium by ultrasound-assisted emulsification microextraction. *J. Chemom.* 2019, *33*.
105. Oktay E., Yayli A. Physical properties of thorium oxalate powders and their influence on the thermal decomposition. *J. Nucl. Mater.* 2001, *288*, 76-82.
106. Paik S., Satpati S. K., Singh D. K. A novel approach of precipitation of Ammonium Di -Uranate (ADU) by sonochemical route. *Progress in Nuclear Energy* 2022, *143*.
107. Narasimha Murty B., Balakrishna P., Yadav R. B., Ganguly C. Influence of temperature of precipitation on agglomeration and other powder characteristics of ammonium diuranate. *Powder Technol.* 2001, *115*, 167-183.
108. Stuart W. I., Miller D. J. The nature of ammonium uranates. *J. Inorg. Nucl. Chem.* 1973, *35*, 2109-2111.